Preparation and mechanism of the sintered bricks produced from Yellow River silt and red mud

Hongtao He, Qinyan Yue *, Yuan Su, Baoyu Gao, Yue Gao, Jingzhou Wang, Hui Yu

Shandong Key Laboratory of Water Pollution Control and Resource Reuse, School of Environmental Science and Engineering, Shandong University, Jinan 250100, China

ARTICLE INFO

ABSTRACT

The preparation, characteristics and mechanisms of sintered bricks manufactured by Yellow River silt and red mud were studied. The sintering shrinkage, weight loss on ignition, water absorption and compressive strength were tested to determine the optimum preparation condition. Sintering mechanisms were discussed through linear regression analysis. Crystalline components of raw materials and bricks were analyzed by X-ray diffraction. Leaching toxicity of raw materials and bricks were measured according to sulphuric acid and nitric acid method. Radiation safety of the sintered bricks was characterized by calculating internal exposure index and external exposure index. The results showed that at the chosen best parameters (red mud content of 40%, sintering temperature of 1050 °C and sintering time of 2 h), the best characteristics of sintered bricks could be obtained. The weight loss on ignition of sintered bricks was principally caused by the removal of absorbed water and crystal water. The sintering shrinkage of sintered bricks mainly depended on sodium compounds and iron compounds of red mud. The sintering process made some components of raw materials transform into other crystals having better thermostability. Besides, the leaching toxicity and radioactivity index of sintered bricks produced under the optimum condition were all below standards.

© 2011 Elsevier B.V. All rights reserved.

1. Introduction

Yellow River flows through the loess plateau, taking away a lot of silt, then the silt deposit in the downstream, known as the Yellow River silt (YRS). Large amount of YRS (about 4×10^8 tons per year) distribute in the lower Yellow River, and the riverbed on the downstream is continuously elevated, which is very dangerous to residents living nearby the valley [1,2]. Therefore, the comprehensive utilization of YRS is imperative. Some researchers have used YRS to produce wall tile [3], ceramic simple bricks [4], perforated bricks [5] and artificial stone used for flood control [6]. But these products often require high preparation temperature (higher than 1100 °C), and their strength also need to be improved.

Red mud (RM) is a by-product from the alumina industry, and production of 1 ton alumina results in 1.2–2 ton RM [7]. Typically, RM is disposed in landfills, which usually takes up too much land and also leads to other serious environmental problems, such as soil contamination, groundwater pollution and increase of dust content in air [8]. Hence, it is very necessary to manage and reuse RM. In China, about 1×10^7 tons of RM are generated per year, and a continuous increase is expected in the future [9], but only a small part of them has been utilized for glass-ceramics [10], cement [11], land composting [12], sewage treatment [13,14], stabilization material [15], building material and metal recovery [16].

Using RM and YRS as raw materials to produce bricks would be a good option. Because it can maximally (100%) realize comprehensive utilization of solid waste; moreover, there were many alkaline substances in RM [17], which not only can lower the sintering temperature to save energy, but also can help form glassy phase to improve the strength of bricks. However, there have been few studies on this field. The aim of the present research was to investigate the feasibility of manufacturing sintered bricks with YRS and RM, and then to determine the best preparation condition. In addition, the weight loss mechanism and shrinkage mechanism were quantitatively discussed, which would provide important theoretical basis for the future research works about sintered bricks.

2. Materials and methods

2.1. Raw materials

YRS was obtained from the edge of the Yellow River, Jinan, China; and RM was obtained from Shandong Aluminum Company, China, which was produced by Bayer process.

* Corresponding author. Tel.: +86 531 88365258; fax: +86 531 88364513.
E-mail address: qyyue@sdu.edu.cn (Q. Yue).

YRS and RM were dried at 105 °C for 4 h in an electric oven thermostat, and then were crushed to pass sieve No. 100 (the diameter of mesh is 0.154 mm) for subsequent use.

2.2. The preparation of sintered bricks

For the preparation of one specimen, a total amount of 40 g raw materials was applied. YRS and RM were mixed by different weight ratio. After 4 mL water (10% by mass ratio) was injected in, the raw materials were homogenized and then suppressed in a mold (diameter of 50 mm, length of 50 mm) at 20 MPa for one minute to obtain a green body.

Green bodies were placed at room temperature for 24 h for desiccation. The dried specimens were sintered in a SX212-16 high temperature box resistance furnace with a heating rate of 2.5 °C/min from room temperature to the designated temperatures, and then were maintained at the highest temperatures for a designated time to ensure the full agglomeration. Finally, sintered bricks were obtained after cooling down to the room temperature.

2.3. Analysis and methods

2.3.1. Chemical analysis

The chemical components of the YRS and RM were determined by energy dispersive X-ray analysis (EDAX), and PV9100 X-ray energy spectrometer was used during this part.

2.3.2. X-ray diffraction (XRD) analysis

Crystal components of raw materials and sintered bricks were studied by a Rigaku (Japan) D/MAX-rA diffractometer (Cu Kα radiation), which was equipped with a graphite monochromator in the diffracted beam. The measured results were used to analyze crystalline phase evolution.

2.3.3. Thermal analysis

Thermal behavior of YRS and RM were tested to determine sintering temperature by thermogravimetry (TG) and differential scanning calorimetry (DSC), using a Q600 SDT synchronization heat analyzer. Raw materials were heated from room temperature (22 °C) to 1100 °C at a rate of 10 °C/min in air atmosphere.

2.3.4. Microstructure analysis

The microstructures of some sintered bricks were characterized by using a JEOL JSM-7600F scanning electron microscope (SEM), helping to explain sintering mechanism.

2.3.5. Leaching toxicity

Heavy metal elements of raw materials and sintered bricks were leached by solid waste-extraction procedure for leaching toxicity-sulphuric acid and nitric acid method [18]. The concentrations of toxic metal elements in the leachates were determined by ICP-AES (IRIS Intrepid II XSP equipment), and then the results were compared with GB 5085.3-2007 [19] to confirm the safety of sintered bricks to be applied in civil engineering.

2.3.6. Radioactivity

In order to assess radiation safety of the sintered bricks, internal exposure index and external exposure index of the bricks were calculated according to specific activity of radionuclide of raw materials, and then the calculation results were compared with GB 6566-2010 [20].

2.3.7. Characterization of sintered bricks

Some important performance indexes (weight loss on ignition, sintering shrinkage, water absorption and compressive strength) were chosen to characterize the quality of the experimental sintered bricks, and then the optimum preparation condition was determined.

Weight loss on ignition meant the weight loss of bricks during the sintering process. Weight loss on ignition was calculated from Eq. (1). Sintering shrinkage was another important index of sintered bricks. If sintering shrinkage was too high, the bricks were easy to suffer from deformation. Sintering shrinkage was calculated from Eq. (2). Bricks with small water absorption could be more durable and resistant to environmental damage. The water absorption can affect strength and durability of bricks, and it was calculated from Eq. (3). Because the specimens were smaller than common bricks, the compressive strength of sintered bricks was measured via a computer controlled automatic pressure testing machine YAW 4106, and it was calculated from Eq. (4). In order to get accurate test results, two repetitions were made to determine these properties of sintered bricks in this research.

$$\text{WLI} = \frac{\text{WBS} - \text{WAS}}{\text{WBS}} \tag{1}$$

where WLI is for weight loss on ignition; WBS is for weight of specimens before sintering; WAS is for weight of specimens after sintering.

$$\text{SS} = \frac{\text{VBS} - \text{VAS}}{\text{VBS}} \tag{2}$$

where SS is for sintering shrinkage; VBS is for volume of specimens before sintering; VAS is for volume of specimens after sintering.

$$\text{WA} = \frac{\text{WASW} - \text{WBSW}}{\text{WBSW}} \tag{3}$$

where WA is for water absorption; WASW is for weight of specimens after soaking in water for 24 h; WBSW is for weight of specimens before soaking in water.

$$\text{CS} = \frac{\text{FB}}{\text{FA}} \tag{4}$$

where CS is for compressive strength; FB is for force of breaking specimens; FA is for force area of specimens

3. Results and discussion

3.1. Analysis on the raw materials

3.1.1. Chemical analysis (EDAX)

The chemical components of YRS and RM are shown in Table 1. It can be seen that silicon and aluminum were the main compositions for YRS, while iron, silicon, aluminum and sodium were major in RM. Because manufacturing perforated bricks with YRS has been a mature technology [21], the similarity between compositions of YRS and RM indicated that preparing bricks with these two materials was possible. The mass ratio of Na_2O in RM was about 14.5%, and the melting points of sodium compounds were relatively low. So mixing RM and YRS to prepare sintered bricks would be a double-win choice, because it not only can decrease the sintering temperature and energy cost, but also can utilize large amount of RM, turning solid waste into resource.

3.1.2. Crystal components analysis (XRD)

The crystal components of YRS were concise as Fig. 1(a) shown, the main component was quartz (SiO_2), and there were a little anorthite ($CaAl_2Si_2O_8$), calcite ($CaCO_3$), illite ($K_{0.7}Al_2(Si,Al)_4O_{10}(OH)_2$) and ($Co_5Zn_{21})_{52}B$. Fig. 1(b) shows that the crystal components of RM were multitudinous, and the main crystalline phases were goethite (α-FeO(OH)), hematite (Fe_2O_3), $Na_5Al_3CSi_3O_{15}$, quartz (SiO_2) and calcite ($CaCO_3$). The XRD analysis results were associated to the chemical components of YRS and RM as Table 1 shown.

Table 1
The chemical components of YRS and RM (%).

	SiO$_2$	Al$_2$O$_3$	Fe$_2$O$_3$	CaO	TiO$_2$	MgO	Na$_2$O	K$_2$O	MnO
YRS	74.01	12.15	3.31	4.12	0.19	2.65	1.90	1.59	0.09
RM	26.36	23.97	30.11	2.58	2.48	–	14.50	–	–
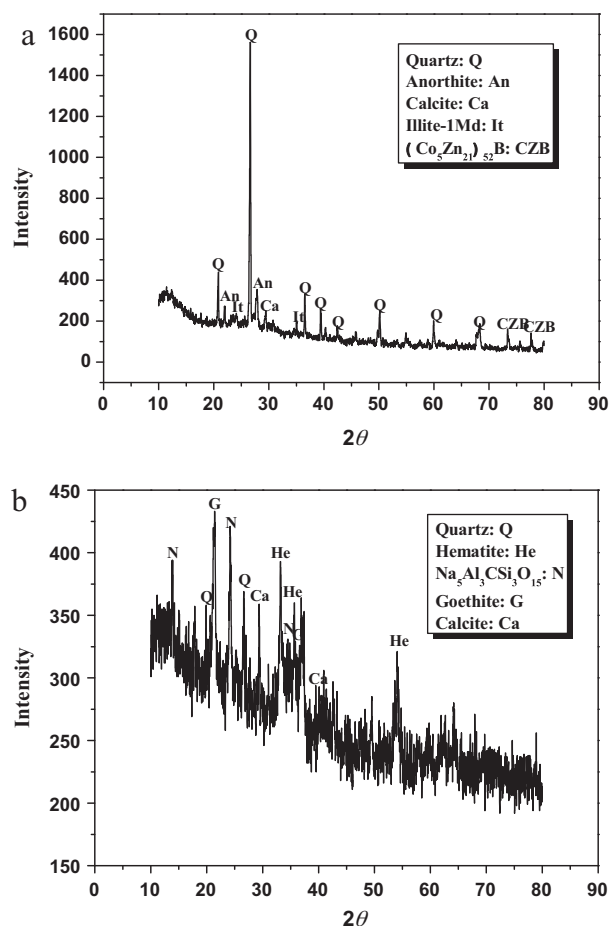
Fig. 1. XRD patterns of YRS (a) and RM (b).

Fig. 2. Thermal analysis of YRS (a) and RM (b), TG: thermogravimetry, DSC: differential scanning calorimetry.

3.1.3. Thermal analysis (TG/DSC)

As Fig. 2(a) shown, there was a continuous weight loss distributed between 28.63–706.07 °C in the TG plot of YRS. The weight loss of 1.682% at 28.63–344.70 °C was attributed to the evaporation of adsorbed water. The weight loss of 4.098% at 344.70–706.07 °C was caused by the release of constitution water from illite (K$_{0.7}$Al$_2$(Si,Al)$_4$O$_{10}$(OH)$_2$). Between 706.07 °C and 934.66 °C, there was almost no weight loss or increase. However, another weight loss of 0.2352% was observed at 934.66–1088.13 °C, due to the decomposition of some crystals. The DSC curve of YRS was comparative smooth, and there were no obvious endothermic peaks.

For RM, as Fig. 2(b) shown, weight loss was more obvious than that of YRS, and the DSC curve was fluctuant. Weight loss of 8.815% at 22–340.42 °C was observed in the TG curve, caused by the removal of adsorbed water. Weight loss of 2.524% at 340.42–655.25 °C was mainly due to the elimination of crystal water. However, when the temperature rose from 655.25 °C to 1089.64 °C, weight increase of 1.094% was observed, which indicated that air reacted with RM at high temperature. Endothermic peaks at around 290.47 °C and 641.62 °C in the DSC curve were caused by the elimination of adsorbed water and crystal water, respectively, which confirmed the analysis results from TG curve.
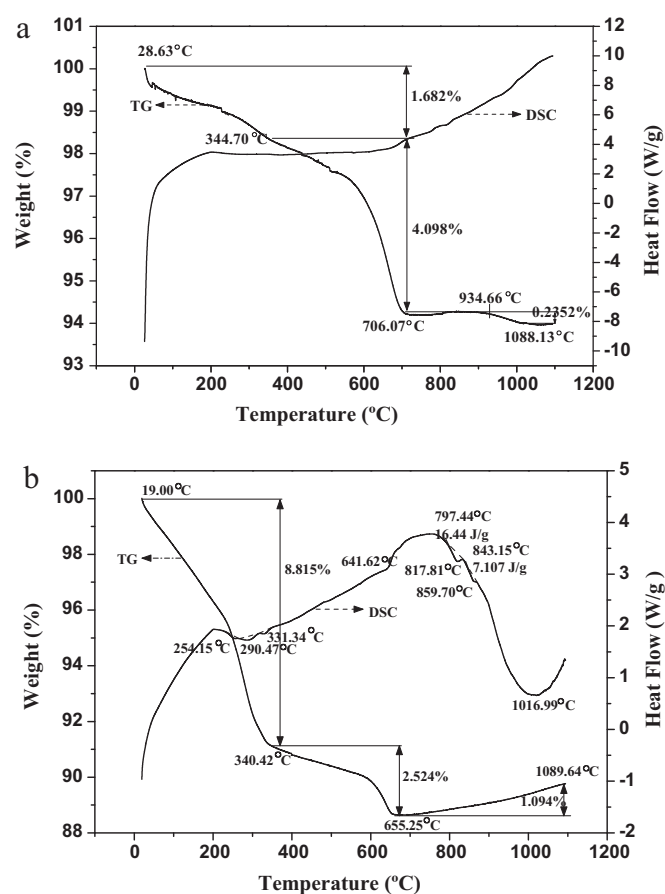
Another two obvious endothermic peaks (817.81 °C and 859.80 °C) should be attributed to the decomposition of calcite [22]. In addition, there was a big endothermic peak at 1016.99 °C, which indicated that the reaction occurring between air and RM at high temperature was endothermic.

It was summarized that YRS can be considered as an inert component below 950 °C. RM also was substantially stable below 900 °C, and the losses of H$_2$O from hydroxide and CO$_2$ from calcite were the only detectable effects, which were in agreement with the analysis results from Sglavo [23].

3.2. Preliminary determination of sintering temperature

In order to obtain solid bricks, adsorbed water and crystal water must be removed and glassy phase should be produced. Below 950 °C, YRS and RM were almost inert. The decomposition reactions of YRS began at 940 °C and basically finished at about 1000 °C (TG plot no longer continued to decline as Fig. 2(a) shown). In addition, synthetic reactions between air and RM began at around of 1017 °C as Fig. 2(b) shown. So 1000 °C was selected as the initial sintering temperature for subsequent experiments.
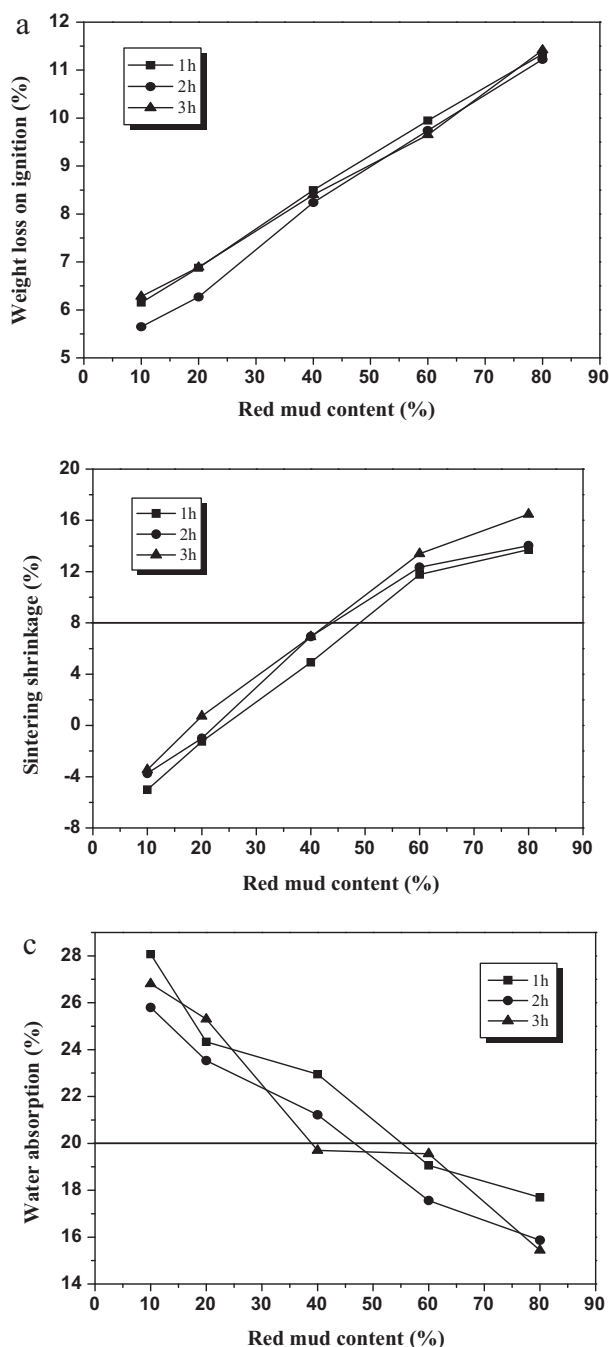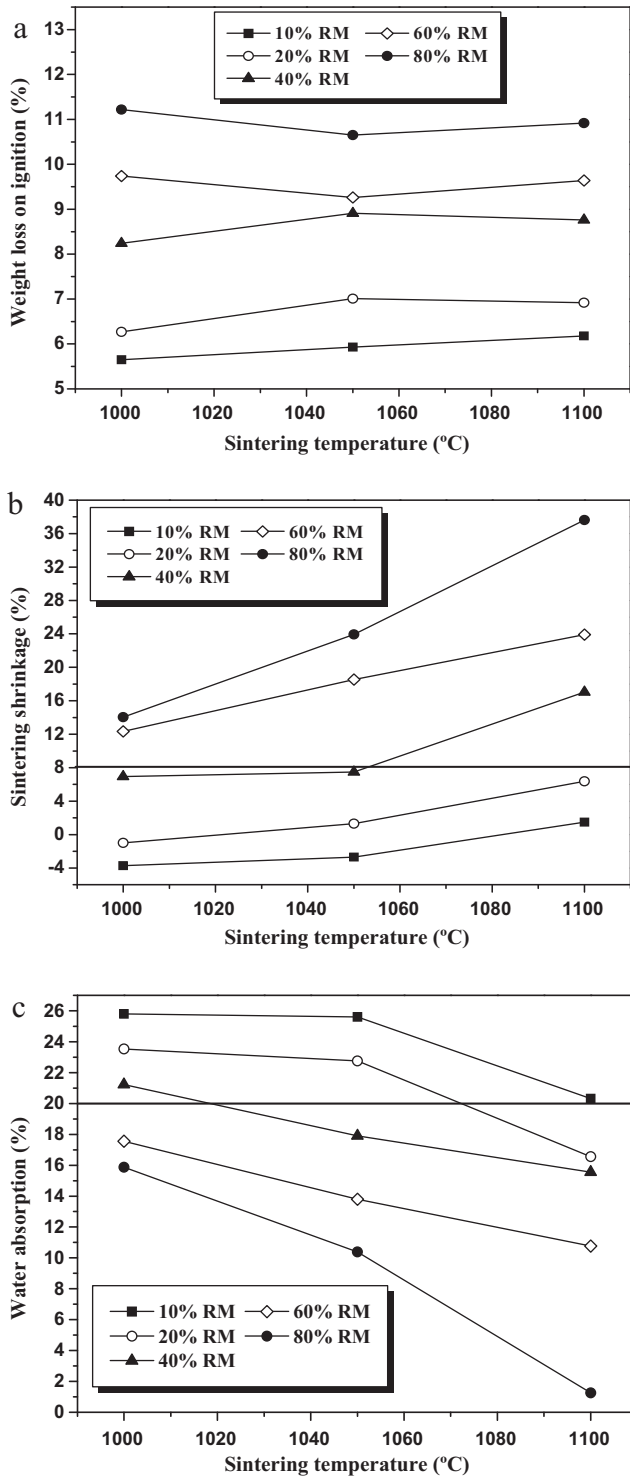
Fig. 3. The characteristics of bricks sintered at 1000 °C for 1 h, 2 h and 3 h; (a) weight loss on ignition, (b) sintering shrinkage, (c) water absorption.

3.3. Determination of the optimum preparation condition

3.3.1. The effect of sintering time and RM content on the properties of bricks

Three groups of samples with different RM content were prepared, and then were sintered at 1000 °C for 1 h, 2 h and 3 h, respectively. There were many dregs falling off from these experimental sintered bricks, especially for the bricks sintered at 1000 °C for 1 h.

Weight loss on ignition, sintering shrinkage and water absorption of the sintered bricks were tested, and the results are presented in Fig. 3. For bricks with the same RM content, the value of these three performance indexes all changed little with the variation of sintering time, meaning that sintering time was not a key factor.

However, for bricks with the same sintering time, when the RM content increased from 10% to 80%, weight loss on ignition obviously increased (about from 6% to 11%) as Fig. 3(a) shown; sintering shrinkage also significantly grew (about from −4% to 14%) as shown in Fig. 3(b); but water absorption decreased about from 27% to 16% as Fig. 3(c) shown, for the increase of sintering shrinkage would lower porosity, and then decrease water absorption of sintered bricks.

3.3.2. The effect of sintering temperature on the properties of bricks

Three groups of samples were sintered at 1000 °C, 1050 °C and 1100 °C for 2 h, respectively. The measured results of weight loss on ignition, sintering shrinkage and water absorption are shown in Fig. 4. For bricks with the same RM content, weight loss on ignition changed little with the variation of sintering temperatures as Fig. 4(a) shown; when sintering temperature rose, sintering shrinkage would observably increase as Fig. 4(b) shown; however, the variation tendency of water absorption was just the opposite as Fig. 4(c) shown, decreasing with the sintering temperature rising.

Normally, for a good clay brick, weight loss on ignition is not more than 15%; sintering shrinkage should be less than 8% [24]; water adsorption should be less than 20% [25]. According to these requirements, bricks produced under two conditions were suitable. The first one: RM content was 40% and sintering temperature was 1050 °C. The second one: RM content was 20% and sintering temperature was 1100 °C. However, the second condition would consume more energy (1100 °C), and the utilization rate of RM was relatively low. In order to maximally realize the RM resource and save energy, the first condition (RM content of 40%, sintering temperature of 1050 °C and sintering time of 2 h) was preferable.

3.3.3. The test of compressive strength

Two experimental bricks with RM content of 40% were sintered at 1050 °C for 2 h, and then their compressive strengths were tested. According to GB5101-2003, minimum compressive strength value of clay bricks with strength grade of MU 30 was 30 MPa. As Table 2 shown, the mean value of compressive strength of the two experimental sintered bricks was 39.1 MPa, which indicated that the sintered bricks were suitable to be used as substitutes of clay bricks.

So the optimum preparation condition was determined as RM content of 40%, sintering temperature of 1050 °C and sintering time of 2 h. The sintering temperature was lower than that of bricks produced only using YRS [4,5], proving that RM can really decrease the sintering temperature of bricks.

3.4. Sintering mechanisms

Sintering mechanisms consisted of weight loss mechanism and shrinkage mechanism. Ten samples (RM content was 5%, 10%, 20%, 30%, 40%, 50%, 60%, 70%, 80% and 90%, respectively) were sintered at 1050 °C for 2 h. Then their weight loss on ignition and sintering shrinkage were measured to discuss the weight loss mechanism and shrinkage mechanism, respectively.

3.4.1. Weight loss mechanism

In order to determine the main reason causing weight loss, the data of weight loss on ignition were analyzed by unary linear regression as line (a) of Fig. 5 shown. The related coefficient was 0.97792, therefore, we could consider that weight loss on ignition was unary linear related to RM content.

According to the thermal analysis of raw materials in Fig. 2, the mass ratio of water in RM was about 11.339% (8.815% adsorbed water and 2.524% crystal water), and that was 5.780% (1.682% adsorbed water and 4.098% crystal water) in YRS. During the experiments, it was found that the weight of dried specimens was near

Table 2
Compressive strength of bricks sintered at 1050 °C for 2 h with 40% RM.

Samples	Area under pressure (mm²)	Breaking force (KN)	Compressive strength (MPa)	Mean value (MPa)
1	1901.17	69.7	36.7	39.1
2	1901.17	78.7	41.4	
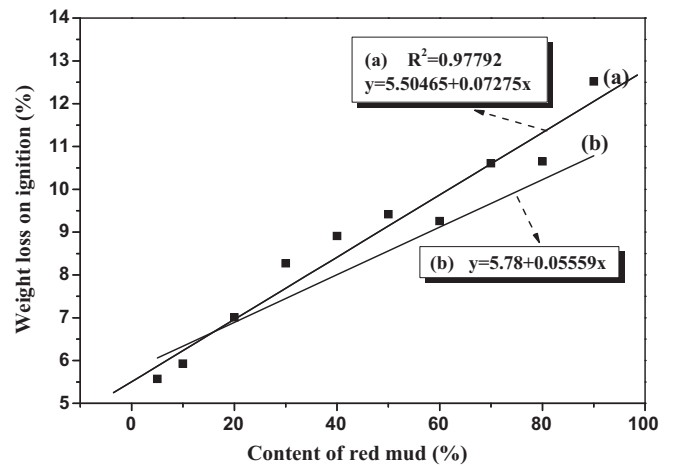
Fig. 5. Weight loss mechanism analysis: (a) weight loss on ignition of bricks sintered at 1050 °C for 2 h; (b) the theoretical water content of dried specimens.

to the weight of raw materials. So it can be supposed that the 4 mL water injected for forming green body had been completely removed through desiccation process (24 h at room temperature), therefore, the theoretical water content (adsorbed water and crystal water) of dried specimens with different RM addition can be calculated from Eq. (5), and the calculation results are shown in the line (b) of Fig. 5. The intercept and slope of line (b) reflected the water content of YRS and the growth rate of theoretical water content with RM content increasing, respectively.

$$Y_1 = 5.78\% + 5.559\%X_1 \tag{5}$$

where Y_1 is for the theoretical water content of dried specimens; X_1 is for the RM content of dried specimens.

As Fig. 5 shown, there were great similarities between line (a) and line (b). Therefore, it can be conjectured that weight loss on ignition was mainly caused by the removal of adsorbed and crystal water of dried specimens. The intercepts of the two lines were approximately equal (5.50465 for line (a), 5.78 for line (b)). However, there was a little difference between their slopes (0.07275 for line (a), 0.05559 for line (b)). Because RM had good water retention property [26], and as the growth of RM content, more water was maintained in the dried specimens to cause the weight increase of the specimens before sintering (dried specimens), so weight loss on ignition would also rise according to Eq. (1). Therefore, weight loss rate was higher than the growth rate of the theoretical water content, in other words, the slope of line (a) was greater than that of line (b).

In addition, from Fig. 4(a), it was found that weight loss on ignition only slightly changed (±0.74%) as the sintering temperature increasing. This can further confirm the above conjecture that weight loss on ignition was mainly caused by the removal of adsorbed and crystal water, and they would be completely eliminated no matter the temperature was 1000 °C, 1050 °C or 1100 °C.

3.4.2. Shrinkage mechanism

The chemical components of ceramic bodies can be classified into three groups: (1) the skeleton components, which formed the

Fig. 4. The characteristics of bricks sintered at 1000 °C, 1050 °C and 1100 °C for 2 h; (a) weight loss on ignition, (b) sintering shrinkage, (c) water absorption.

framework and surfaces of ceramic bodies, mainly consisting of SiO_2 and Al_2O_3; (2) the flux materials, which lowered the melting point, mainly containing alkali metal oxide and alkaline-earth metal oxide such as CaO, Na_2O, K_2O and MgO; (3) the gaseous components, which generated gases and bloated the ceramic bodies in the sintering process at high temperature, mainly containing Fe_2O_3 [27]. Sintering shrinkage of bricks depended on the flux materials and the gaseous components. The former could produce molten materials to compress interspaces, and the latter could release gases to expand pore.

As Table 1 shown, the weight percent of SiO_2 and Al_2O_3 in YRS was about 74.01% and 12.15%, respectively, which meant that more than 86% of the weight of YRS was the skeleton components and YRS was thermostable. However, the skeleton components, flux materials and gaseous components all were found in RM, and their weight percent was about 50% (SiO_2 and Al_2O_3), 30% (Fe_2O_3) and 14.5% (Na_2O), respectively. From Fig. 1(b), it can be seen that the main components of RM were goethite (α-FeO(OH)), hematite (Fe_2O_3), $Na_5Al_3CSi_3O_{15}$, quartz (SiO_2) and calcite ($CaCO_3$). When the temperature grew from room temperature to 1050 °C, calcite and hematite decomposed at 800 °C and more than 1000 °C, respectively, as Eqs. (6) and (7) shown [28]. However, the volume of CO_2 was very small due to the low mass fraction of $CaCO_3$, which meant O_2 was the main gases during sintering process. So the amount of molten materials depended on sodium compounds of RM, while the volume of gases mainly hinged on iron compounds of RM.

$$CaCO_3 \rightarrow CaO + CO_2 \uparrow \tag{6}$$

$$3Fe_2O_3 \rightarrow 2Fe_3O_4 + \frac{1}{2}O_2 \uparrow \tag{7}$$

At high temperature, if O_2 was wrapped in molten materials, the volume of bricks would expand. However, as Fig. 6 shown, most of bricks shrank, and shrinking value rose from −4.47% to 25.64% as RM content increased from 5% to 90%. This indicated that there had been lot of little interspaces in the inside of dried specimens before sintering operation, and the volume fraction of these little interspaces would be slightly increased, corresponding to the removal of adsorbed water and crystal water during sintering process. When the temperature was up to 1050 °C, molten materials would fill these little interspaces. So, sintering shrinkage can be simply calculated from Eq. (8).

$$Y_2 = (A - B) \times X_2 - Z = C \times X_2 - Z \tag{8}$$

where Y_2 is for sintering shrinkage of bricks; X_2 is for RM content; A is for the flux materials coefficient reflecting the effect of sodium compounds of RM on sintering shrinkage; B is for the gases coefficient reflecting the effect of iron compounds of RM on sintering shrinkage; C is for the coefficient colligating A and B; and Z is for the increment of volume percent of the original little interspaces during sintering process.
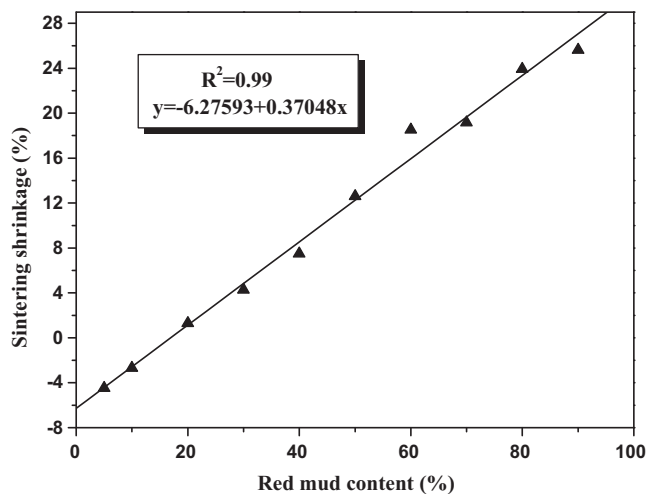

Fig. 6. Shrinkage mechanism analysis: sintering shrinkage of bricks sintered at 1050 °C for 2 h.

The data of sintering shrinkage were fitted by unary linear regression, and related coefficient was 0.99. This meant there was remarkable positive correlativity between RM content and sintering shrinkage, confirming the correctness of Eq. (8). The intercept and slope of the fitted straight line was −6.27593 and 0.37048, respectively. Therefore, the increment of volume percent of the original little interspaces during sintering process was about 6.27593%, and the colligation influence coefficient of RM was about 0.37048.

3.5. Microstructures analysis of sintered bricks

SEM photographs of the fracture surface of bricks sintered at 1050 °C for 2 h are shown in Fig. 7. It can be seen that as the RM content rising from 5% to 80%, more glassy phases were observed and the number of small holes was reduced. Because when RM content increase, more molten materials would be produced owing to the growth of flux materials, which would form more glassy phases and compress the internal space of sintered bricks [29,30]. Especially for sintered bricks with RM content of 5%, as Fig. 7(a1) shown, internal particles did not stick together and there were still lot of original little interspaces, due to lack of enough flux materials. The microstructures were consistent with the growth trend of sintering shrinkage in Fig. 6.

3.6. Leaching toxicity

To inspect and compare the leaching toxicity of YRS, RM and sintered bricks prepared in the optimum condition, heavy metals
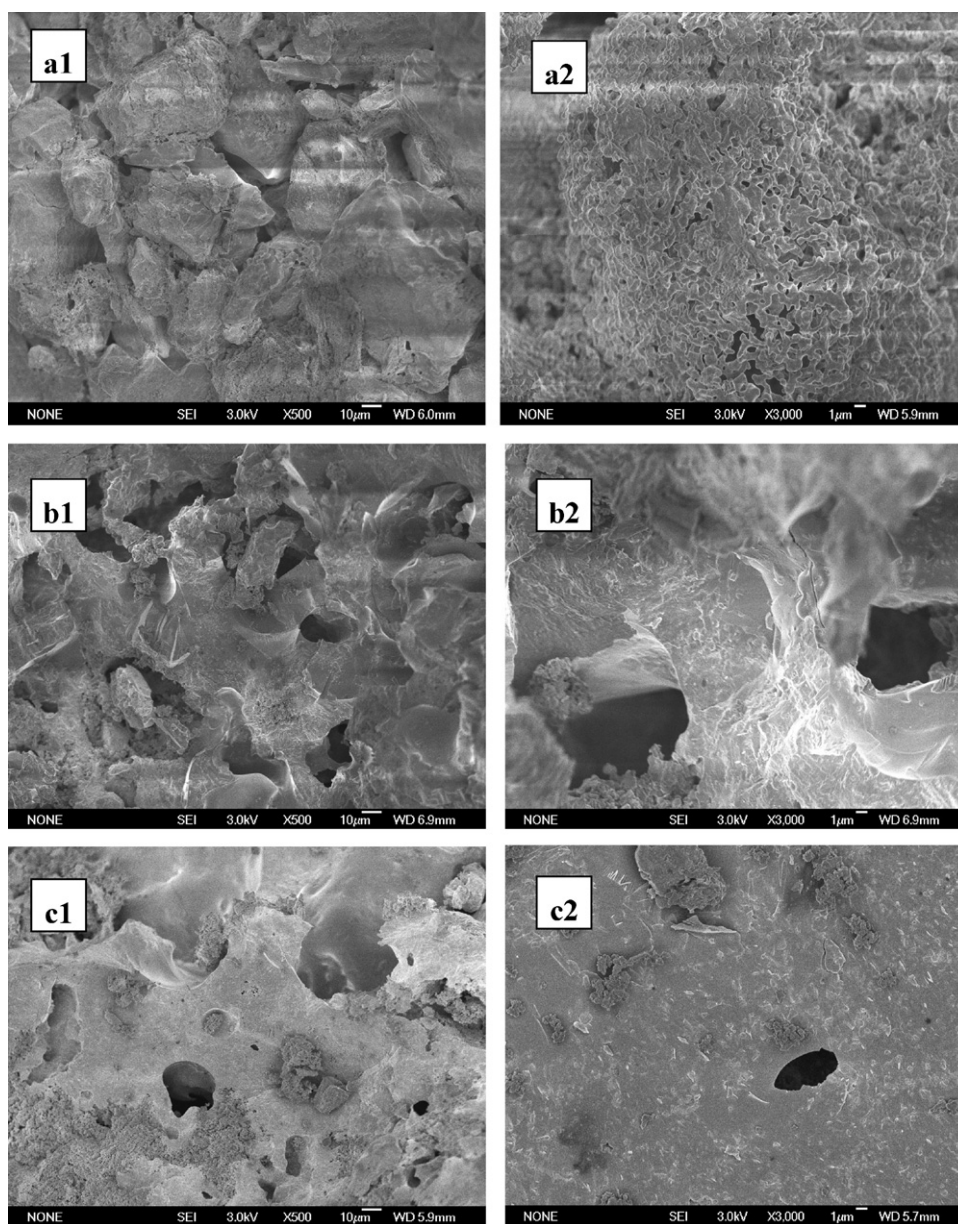
Table 3
Concentrations of toxic metal elements in the leachates of YRS, RM and sintered bricks prepared in the optimum condition (mgL^{-1}).

Toxic metal elements	Ba	Cr	Cu	Ni	Pb	Zn	As	Cd	Co
Concentrations in the leachates of YRS	0.069	1.108	0.176	N	0.108	0.083	N	N	N
Concentrations in the leachates of RM	0.120	8.814	2.844	1.062	0.821	3.134	0.190	N	N
Theoretical concentrations in the leachates of sintered bricks (40% RM and 60% YRS)	0.089	4.190	1.243	0.425	0.393	1.303	0.076	N	N
Concentrations in the leachates of sintered bricks	0.040	1.585	0.198	0.124	0.090	0.178	0.245	N	N
Toxicity thresholds	100	15	100	5	5	100	5	1	–

Fig. 7. SEM photographs showing fracture surface of bricks sintered at 1050 °C for 2 h (RM content of 5% – 500 times (a1), 3000 times (a2); RM content of 40% – 500 times (b1), 3000 times (b2); RM content of 80% – 500 times (c1), 3000 times (c2)).

(Ba, Cr, Cu, Ni, Pb, Zn, As, Cd and Co) in the leachates were measured and their concentrations are shown in Table 3. As can be seen, for YRS, RM and bricks, all heavy metal contents in leachates did not exceed threshold prescribed in GB5085.3-2007, of which, the concentrations of Cd and Co were lower than detection limit. However, the concentrations of heavy metals (except As) in the leachates of sintered bricks were far less than theoretical concentrations, which indicated that sintering process had good immobilization effect on the heavy metals [2].

3.7. Radioactivity

According to national standard GB 6566-2010, ^{226}Ra, ^{232}Th and ^{40}K were used to assess radiation safety of building materials. Because of limited experimental condition, specific activity of radionuclide in RM was provided by Shandong Aluminum Company where RM used in our study were produced; specific activity

Table 4
Specific activity of radionuclide in YRS and RM (Bq kg^{-1}).

	^{226}Ra	^{232}Th	^{40}K
YRS	41.4	56.9	623.9
RM	59.83	293.81	10

of radionuclide in YRS was obtained from Li and Xie' research work [31].

Specific activity of ^{226}Ra, ^{232}Th and ^{40}K in YRS and RM are presented in Table 4. Internal exposure index and external exposure index were calculated from Eqs. (9) and (10), respectively, and the two indexes of main materials for building must be less than 1 in accordance with GB 6566-2010.

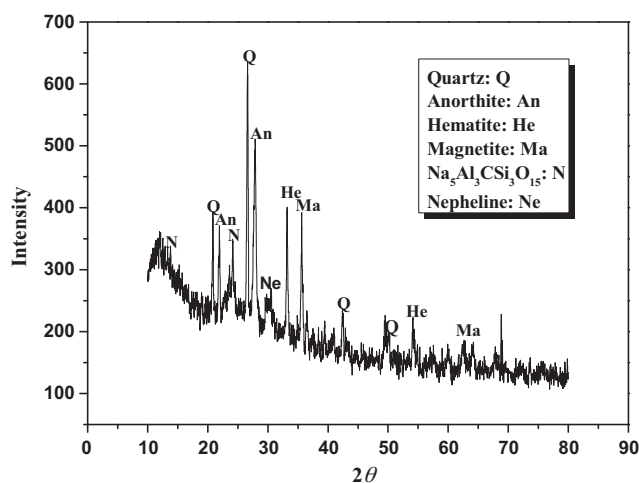$$I_{Ra} = \frac{C_{Ra}}{200Bq \cdot kq^{-1}} \tag{9}$$

Fig. 8. XRD patterns of sintered bricks produced under the optimum condition.

$$I_r = \frac{C_{Ra}}{370 \ \text{Bq} \ \text{kg}^{-1}} + \frac{C_{Th}}{260 \ \text{Bq} \ \text{kg}^{-1}} + \frac{C_K}{4200 \ \text{Bq} \ \text{kg}^{-1}} \qquad (10)$$

where I_{Ra} and I_r are for internal exposure index and external exposure index, respectively; C_{Ra}, C_{Th} and C_K are for specific activity of ^{226}Ra, ^{232}Th and ^{40}K, respectively ($\text{Bq} \ \text{kg}^{-1}$).

By calculation, internal exposure index and external exposure index of YRS was 0.21 and 0.48, respectively; while internal exposure index and external exposure index of RM was 0.30 and 1.29, respectively. The radiation level of bricks can be calculated on the basis of the proportion of raw materials [32]. Therefore, the theoretical internal exposure index and external exposure index of the sintered bricks produced under the best preparation condition (RM content of 40%) was 0.246 and 0.804, respectively.

The leaching toxicity and radioactivity index of sintered bricks produced under the optimum condition were all below standards. Consequently, it was harmless and safe to use them as construction materials.

3.8. XRD analysis of sintered bricks produced under the optimum condition

As Fig. 8 shown, the main crystal components of the sintered bricks produced under the optimum condition were quartz (SiO_2), anorthite ($CaAl_2Si_2O_8$), hematite (Fe_2O_3), magnetite (Fe_3O_4), $Na_5Al_3CSi_3O_{15}$ and a little nepheline ($NaAlSiO_4$). Comparing with Fig. 1(a) and (b), it can be seen that the amount of anorthite increased, goethite and calcite disappeared, and magnetite and nepheline were observed for the first time. The extinction of goethite and calcite was due to their decomposition at high temperature, and the decomposition product of calcite, CaO, contributed to the increase of anorthite. At 1050 °C, a part of hematite could transform to magnetite as Eq. (7) shown. The appearance of a little nepheline might be caused by illite decomposing. All in all, through the sintering operation, the unstable substances with poor thermal stability would be transformed to other thermostable substances [33,34].

4. Conclusions

In this study, the optimum condition for preparing sintered bricks with YRS and RM was determined as follow: RM content was 40% by mass ratio; the sintering temperature was 1050 °C; the sintering time, a non-critical factor, was 2 h. Under the best preparation condition, weight loss on ignition, sintering shrinkage, water absorption and compressive strength of the sintered bricks

were 8.91%, 7.49%, 17.91% and 39.1 MPa, respectively, meeting the requirements of common bricks. And according to the toxic metal leaching test results and the calculation results of internal and external exposure index, the sintered bricks were safe to the environment. Therefore, it was quite feasible to manufacture sintered bricks with YRS and RM.

Comparing the results from calculation and experiments, it was found that weight loss on ignition was essentially caused by the removal of adsorbed water and crystal water. Sintering shrinkage mainly depended on sodium compounds (flux materials) and iron compounds (gaseous components) of RM. The comparative analysis on XRD patterns of raw materials and sintered bricks produced under the optimum condition indicated that high temperature can make substances with poor thermal stability transform to other substances with good thermal stability.

References

[1] Z.L. Wei, A little management strategy about the lower Yellow River, Yellow River 6 (2004) 17–18.
[2] W.J. Wang, The thinking on the lower Yellow River management, China Water Resour. 11 (2004) 26–28.
[3] J.S. Zhang, G. Feng, W.H. Wu, C.M. Han, X.R. Zhang, Producing wall and floor tiles by using the Yellow River sediment, China Build. Mater. Sci. Technol. 4 (1996) 38–41.
[4] J.F. Wu, D.K. Deng, X.H. Xu, G.H. Leng, Research on the preparation of ceramic simple brick made from Yellow River silt, Sci. Technol. 2 (2009) 35–37.
[5] H. Li, H. Zhang, F.S. Zhang, The discussion on application of the Yellow River silt sintered porous bricks, Wall Mater. Innovat. Energy Sav. Build. 10 (2006) 29–32.
[6] J.P. Zhang, R.L. Li, L. Zhang, J.S. Zhang, The bright prospect of using Yellow River silt to produce the artificial stone, Shandong Build. Mater. 1 (2007) 12–15.
[7] R.U. Ayres, H. John, A. Bjom, Utilisation of the wastes in New Millennium, Mrs. Bull. 7 (2001) 477–480.
[8] J.F. Wu, W.H. Luo, X.H. Xu, F.X. Teng, Preparation of the thermal insulating red mud ceramic bricks and its microstructure and performance, J. Wuhan Univ. Technol. 30 (2008) 15–18.
[9] S. Zhang, C. Liu, Z. Luan, X. Peng, H. Rena, J. Wang, Arsenate removal from aqueous solutions using modified red mud, J. Hazard. Mater. 152 (2008) 486–492.
[10] J.K. Yang, D.D. Zhang, J. Hou, B.P. He, B. Xiao, Preparation of glass–ceramics from red mud in the aluminium industries, Ceram. Int. 34 (2008) 125–130.
[11] P.E. Tsakiridis, S. Agatzini-Leonardou, P. Oustadakis, Red mud addition in the raw meal for the production of Portland cement clinker, J. Hazard. Mater. B116 (2004) 103–110.
[12] E. Lombi, F.J. Zhao, G. Wieshammer, G. Zhang, S.P. McGrath, In situ fixation of metals in soils using bauxite residue: biological effects, Environ. Pollut. 118 (2002) 445–452.
[13] V.K. Gupta, I. Ali, V.K. Saini, Removal of chlorophenols from wastewater using red mud: an aluminum industry waste, Environ. Sci. Technol. 38 (2004) 4012–4018.
[14] H. Nadaroglu, E. Kalkan, N. Demir, Removal of copper from aqueous solution using red mud, Desalination 251 (2010) 90–95.
[15] E. Kalkan, Utilization of red mud as a stabilization material for the preparation of clay liners, Eng. Geol. 87 (2006) 220–229.
[16] W.C. Liu, J.K. Yang, B. Xiao, Application of Bayer red mud for iron recovery and building material production from alumosilicate residues, J. Hazard. Mater. 161 (2009) 474–478.
[17] Y. Liu, C.X. Lin, Y.G. Wu, Characterization of red mud derived from a combined Bayer Process and bauxite calcination method, J. Hazard. Mater. 146 (2007) 255–261.
[18] State Environmental Protection Administration of China, HJ/T299-2007, Solid Waste-Extraction Procedure for Leaching Toxicity-Sulphuric acid & Nitric Acid Method, China Environmental Science Press, Beijing, 2007.
[19] State Environmental Protection Administration of China, GB 5085. 3-2007, Identification Standards for Hazardous Wastes-Identification for Extraction Toxicity, China Environmental Science Press, Beijing, 2007.
[20] State Administration for Quality Supervision and Inspection and Quarantine of China, GB 6566-2010, Limits of Radionuclides in Building Materials, China Standards Press, Beijing, 2010.
[21] Z.J. Hu, Discussion of the techniques of multi-hollow bricks used the silt from Huanghe River, Shandong Build. Mater. 1 (2002) 18–20.

[22] V.M. Sglavo, R. Campostrini, S. Maurina, G. Carturan, M. Monagheddu, G. Budroni, G. Cocco, Bauxite, 'red mud' in the ceramic industry. Part 1. Thermal behaviour, J. Eur. Ceram. Soc. 20 (2000) 235–244.

[23] V.M. Sglavo, S. Maurina, A. Conci, A. Salviati, G. Carturan, G. Cocco, Bauxite, 'red mud' in the ceramic industry. Part 2. Production of clay-based ceramics, J. Eur. Ceram. Soc. 20 (2000) 245–252.

[24] P.H. Shih, Z.Z. Wu, H.L. Chiang, Characteristics of bricks made from waste steel slag, Waste Manage. 24 (2004) 1043–1047.

[25] General Administration of Quality Supervision Inspection and Quarantine of China, GB 5101-2003, Fired Common Bricks, China Standard Press, Beijing, 2003.

[26] Y.R. Jing, Q. Yang, Y.Q. Jing, Basic properties of red mud and engineering characteristics of it, Shanxi Architect. 27 (2001) 80–82.

[27] Y.F. Qi, Q.Y. Yue, S.X. Han, M. Yue, B.Y. Gao, H. Yu, T. Shao, Preparation and mechanism of ultra-lightweight ceramics produced from sewage sludge, J. Hazard. Mater. 176 (2009) 76–84.

[28] Y. Pontikes, C. Rathossi, P. Nikolopoulos, G.N. Angelopoulos, D.D. Jayaseelan, W.E. Lee, Effect of firing temperature and atmosphere on sintering of ceramics made from Bayer process bauxite residue, Ceram. Int. 35 (2009) 401–407.

[29] G.R. Xu, J.L. Zou, G.B. Li, Ceramsite obtained from water and wastewater sludge and its characteristics affected by $(Fe_2O_3 + CaO + MgO)/(SiO_2 + Al_2O_3)$, Water Res. 43 (2009) 2885–2893.

[30] J.L. Zou, G.R. Xu, G.B. Li, Ceramsite obtained from water and wastewater sludge and its characteristics affected by Fe_2O_3, CaO, and MgO, J. Hazard. Mater. 165 (2009) 995–1001.

[31] R.X. Liu, X.J. Xie, The study on the radioactivity level of Yellow River silt porous brick, China Sci. Technol. Panorama Mag. 12 (2009) 8.

[32] S. János, J. Viktor, K. József, T. Sándor, K. Tibor, Radiological aspects of the usability of red mud as building material additive, J. Hazard. Mater. 150 (2008) 541–545.

[33] M. Romero, A. Andrés, R. Alonso, J. Viguri, J.Ma. Rincón, Sintering behaviour of ceramic bodies from contaminated marine sediments, Ceram. Int. 34 (2008) 1917–1924.

[34] M.S. El-Mahllawy, Characteristics of acid resisting bricks made from quarry residues and waste steel slag, Constr. Build. Mater. 22 (2008) 1887–1896.